

# Performance analysis of DFT-S-OFDM waveform for Li-Fi systems

S. Hussin<sup>a</sup>, E. Mansour Shalaby<sup>b\*</sup>

<sup>a</sup> Electronics and Communication Engineering Department, Faculty of Engineering, Zagazig University, Zagazig, 44519 Egypt

<sup>b</sup> Electrical Engineering & Computers Department, Higher Technological Institute, 10<sup>th</sup> of Ramadan City, Megawra 1, 44629 Egypt

## Article info

### Article history:

Received 03 Aug 2021

Received in revised form 16 Oct. 2021

Accepted 18 Oct. 2021

Available on-line 29 Nov. 2021

### Keywords:

Light-fidelity, visible light communications, orthogonal frequency division multiplexing, discrete Fourier transform spread, peak-to-average power ratio.

## Abstract

In this paper, the effect of an indoor visible light communication channel is studied. Moreover, the analysis of the received power distribution of the photodiode in the line of sight and the first reflection of the channel without line of sight with several parameters is simulated. Two different waveforms are explained in detail. Orthogonal frequency division multiplexing has been widely adopted in radio frequency and optical communication systems. One of the most important disadvantages of the orthogonal frequency division multiplexing signal is the high peak-to-average power ratio. Therefore, it is important to minimize the peak-to-average power ratio in the visible light communication systems more than in radio-frequency wireless applications. In the visible light communication systems, the high peak-to-average power ratio produces a high DC bias which reduces power efficiency of the system. A discrete Fourier transform spread orthogonal frequency division multiplexing is proposed to be used in wireless communication systems; its ability to minimize peak-to-average power ratio has been tested. The analysis of two different subcarrier allocation methods for the discrete Fourier transform-spread subcarriers, as well as the examination of two distinct subcarrier allocation strategies, distributed and localized mapping, are investigated and studied. The effects of an accurate new sub-band mapping for the localized discrete Fourier transform spread orthogonal frequency division multiplexing scheme are presented in this paper. The light-fidelity system performance of the orthogonal frequency division multiplexing and discrete Fourier transform spread orthogonal frequency division multiplexing with different sub-mapping techniques are simulated with Matlab™. A system performance size of bit error rate and peak-to-average power ratio are obtained, as well.

## 1. Introduction

Growth in the number of wireless communication devices in the spectrum bands is more frequent and these bands have become overcrowded. Visible light communication (VLC) is a gifted technique which uses the low-cost of the current lighting infrastructure for wireless optical communication purposes. VLC is a point-to-point optical wireless communication with a high-speed data rate. Light-fidelity (Li-Fi) is a complete VLC system that uses visible

light as a carrier signal. It is a promising candidate for different applications such as internet of things (IOT) and indoor positioning.

The suitable modulation technique for Li-Fi systems is an intensity modulation and direct detection (IM/DD) technique. It converts an electrical signal to an optical signal using a light-emitting diode (LED) as a transmitter. At the receiver, a photo detector (PD) converts an optical power signal into an electrical signal. Therefore, since the optical signal intensity is used to modulate the data, the signal is unipolar with only positive values. [1].

A square-law detector can be used to represent the PD. It produces a current impulse by generating a shot noise

\*Corresponding author at: [islam.shalaby@hti.edu.eg](mailto:islam.shalaby@hti.edu.eg)

from incoming photons. The Gaussian distribution can be used to describe the shot noise [2]. The Gaussian distribution is also used to describe the thermal noise generated by the electrical components which are connected to the PD. Single carrier modulation techniques can be easily implemented in Li-Fi systems. Inter-symbol interference (ISI) is caused by the limited bandwidth of the optical wireless communication channel and the limited modulation bandwidth of the front-end devices; hence, a complex equalizer at the receiver is required for high data rates. Therefore, the performance and spectral efficiency of these techniques decrease. On the other hand, the orthogonal frequency division multiplexing (OFDM) is one of the multiple carrier modulation techniques which have been shown as candidates for optical wireless communication channels. A single tap equalizer at the receiver is simply required to achieve high data rates and spectral efficiency [3]. OFDM is a modulation technique which is used in many broadband wired and wireless communication systems. It is used to combat multipath fading by using a cyclic prefix (CP) which reduces the spectral efficiency. In addition, a rectangular impulse response of OFDM symbols has a very important drawback. It allows OFDM to suffer from high side-lobes which produce high out-of-band (OOB) spectra and then, fall slowly. The side-lobes increase the OFDM signal bandwidth and reduce the spectral efficiency. Although, OFDM systems are complex compared to single carrier systems due to the design of their transmitter and receiver, as well as the associated signal processing, significant benefits are achieved. One of disadvantages of the OFDM waveform is its high peak-to-average power ratio (PAPR). Therefore, it is important to minimize PAPR in the VLC systems more than in wireless and optical RF applications. The high PAPR in VLC systems causes a nonlinear signal distortion in the power amplifier, as well as a huge DC bias which decreases the system power efficiency. A discrete Fourier transform spread OFDM (DFT-S-OFDM) is developed to reduce PAPR in wireless communication systems. It allows for a single carrier modulation and frequency domain equalization to be used as seen in the uplink of the 3rd generation partnership project (3GPP) for a 4G long-term evolution (LTE) [4,5]. Because of its single carrier structure, it was proven to be an effective technique for mitigating PAPR. Thus, it is named a single carrier frequency division multiplexing (SC-FDM). The scheme utilizes additional discrete Fourier transforms (DFTs) and inverse discrete Fourier transforms (IDFTs) at the transmitter and receiver to reduce PAPR. It has the disadvantage of increasing computing complexity.

In this paper, an indoor channel modelling for the VLC is discussed in detail. Moreover, the analysis of the received power of the photodiode in the indoor line-of-sight (LoS) and the first reflected channel without line-of-sight (NLoS) of the VLC system is presented. The analysis of the performance of OFDM and DFT-S-OFDM modulation techniques in VLC communication systems using a single LED is investigated.

This paper is organized as follows: section 2 presents the indoor channel modelling for the VLC system. Section 3 describes the OFDM modulation technique with the Hermitian symmetry which is used to produce a real OFDM time domain output signal. In section 4, it is

explained how to use a DFT-S-OFDM approach with different mapping for a sub-band of the DFT-Spread subcarriers. The generation of a real DFT-S-OFDM time domain output signal is discussed. In section 5, the simulation results of the OFDM and DFT-S-OFDM modulation techniques in the VLC system in terms of metrics such as bit error rate (BER), and PAPR at 150 Mbps with a 16-QAM format and a 1024-point FFT using Matlab™ are shown, indicating that the proposed technique reduces PAPR by a significant amount. Finally, conclusions are drawn in section 6.

## 2. VLC system channel model

The communication channel model is one of the most significant factors that defines the efficiency of Li-Fi systems. The channel in the VLC system is a free space which can be classified into LoS and NLoS routes [6,7]. Reflections do not need to be taken into account in the LoS channel situation. And only path loss is determined in these situations based on the knowledge of the distance between source and receiver, receiver size, and transmitter beam divergence. In the NLoS case, leading to reflections on various walls or obstacles, multiple paths should be considered that the optical signal will take from source to receiver. Thus, the estimation of direction loss is more complicated as shown in Fig. 1.

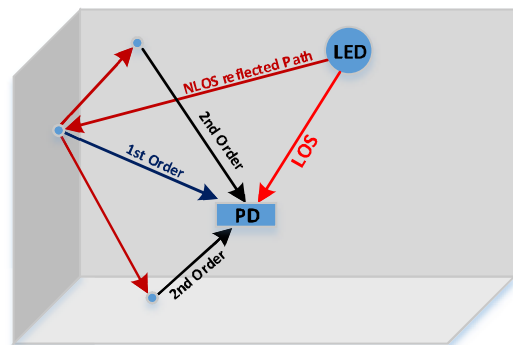


Fig. 1. Free space indoor VLC channel model.

The main component of the received power in the LoS link is power from the LED source. Reflections can be considered as the Lambertian model. The propagation delay varies in the case of LoS and NLoS paths. In the LoS path, the delay for the direct path is expected to be smaller than for the reflected path. In the NLoS path, there is only a propagation delay caused by the reflected signal.

Due to the photodetector pointing upwards and the lower floor reflectivity index, the reflected signal from the area below the receiver cannot reach the photodetector area. Therefore, it is not considered in most simulations.

Visible light components are used for both lighting and wireless data communication. Transmitted signal is modulated by differentiating the optical power which is known as IM. The signal detection is demodulated at the receiver by DD. A linear additive white Gaussian noise (AWGN) channel is used for modelling VLC systems. At the receiver, PD collected photons and converted them into the electric current  $I_{PD}$ . The received optical power value is measured by the equation:

$$P_r = \frac{I_{PD}}{R_{PD}}, \quad (1)$$

where  $R_{PD}$  is the PD responsivity.

The received power can be calculated using the optical wireless communication channel impulse response  $H_{OWC}$  by:

$$P_r = P_t H_{OWC} + N, \quad (2)$$

where  $P_t$  is the transmitted optical power and  $N$  is the AWGN [8,9]. In this paper, the channel model is based on the model implemented by Ref. 10, where the indoor LoS and NLoS optical system propagation path looks as shown in Fig. 2.

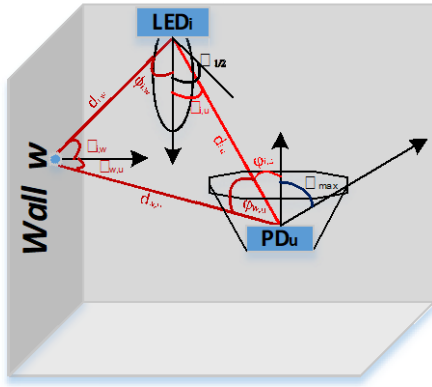


Fig. 2. Indoor VLC system model.

The transmitter is usually an  $LED_i$  mounted on the ceiling of the room directed downwards, perpendicular to the floor, while the receiver, usually a  $PD_u$  photodetector points up towards the transmitter.

A generalized Lambertian radiant intensity was used to model the LED angular distribution of the radiation intensity pattern  $R_0(\phi_{i,u})$  which is given by:

$$R_0(\phi_{i,u}) = \begin{cases} \frac{(m+1)}{2\pi} \cos^m \phi_{i,u}, & \phi_{i,u} \in \left[-\frac{\pi}{2}, \frac{\pi}{2}\right] \\ 0, & \phi_{i,u} \geq \frac{\pi}{2} \end{cases}, \quad (3)$$

where  $\phi_{i,u}$  is the irradiance angle and  $m$  is the order of Lambertian emission which can be expressed by:

$$m = (-\ln 2) / \ln \Phi_{1/2}, \quad (4)$$

where  $\Phi_{1/2}$  is the radiation half-angle at half the intensity of the main beam direction.

The wireless optical channel impulse response is obtained by a recursive algorithm which consists of calculating two components: LoS and NLoS.

The LoS channel transfer function  $H_{LoS}$  is essentially independent of the modulation frequency. Moreover, it is determined by the distance between the transmitter and receiver, as well as their direction in relation to the line of sight. The LoS channel component is expressed in Refs. 11 and 12 by Eq. (5):

$$H_{LoS} = \begin{cases} \frac{A_{PD}}{d_{i,u}^2} R_0(\phi_{i,u}) \cdot g_f \cdot g_c(\psi_{i,u}) \cdot \cos \psi_{i,u}, & 0 \leq \psi_{i,u} < \Psi_{max} \\ 0, & \psi_{i,u} \geq \Psi_{max} \end{cases}, \quad (5)$$

where  $\psi_{i,u}$  is the incidence angle,  $A_{PD}$  is the photo detector area, the LoS path of Li-Fi system which consists of  $LED_i$  and  $PD_u$  is the straight line between them which can be denoted by  $d_{i,u}$ ,  $g_f$  is the optical filter gain, and  $g_c(\psi_{i,u})$  is the optical concentrator gain which is given by:

$$g_c(\psi_{i,u}) = \begin{cases} \frac{n^2}{\sin^2 \Psi_{max}}, & 0 \leq \psi_{i,u} < \Psi_{max} \\ 0, & \psi_{i,u} > \Psi_{max} \end{cases}, \quad (6)$$

where  $n$  indicates the connector refractive index and  $\Psi_{max}$  is the field of view (FOV) half-angle of the PD which has a maximum value of  $\frac{\pi}{2}$ .

Only first-order reflections are considered in the NLoS path for simplicity. A first-order reflection consists of two components: from the LED to a small area  $w$  on the side wall i), and from the side wall  $w$  to the PD ii).

The distances of these components are denoted by  $d_{i,w}$  and  $d_{w,u}$ , respectively. The angles of radiance and incidence corresponding to the first component are  $\phi_{i,w}$  and  $\theta_{i,w}$ , respectively, and for the second part, they are denoted by  $\theta_{w,u}$  and  $\phi_{w,u}$ , respectively. A delay between distinct paths can be ignored because indoor propagation paths are relatively short. In other words, signals with different paths are expected to reach the receiver at the same time.

According to the literature [11,13], inside a room, the first NLoS reflection of an optical source wide-beam emits the intensity  $I_e$  over the entire surface of the room.  $A_{room}$  is given by the equation:

$$I_e = \rho_1 \frac{P_t}{A_{room}}, \quad (7)$$

where  $\rho_1$  is the surface reflectivity and  $P_t$  is the LED power.

The average reflectivity  $\rho_{av}$  is described as:

$$\rho_{av} = \frac{1}{A_{room}} \sum_i \rho_i A_i, \quad (8)$$

where  $\rho_i$  is the walls individual reflectivity by the room windows and other objects which are weighted by their individual areas  $A_i$ .

Therefore, the total received intensity  $I$  is given by summing up the geometrical series:

$$I = I_e \sum_j \rho_{av}^{j-1} = \frac{I_e}{1 - \rho_{av}}, \quad (9)$$

where the index  $j$  is the reflection number.

The PD surface is assumed as a small part of the room surface, so the received NLoS power  $P_{r-NLoS}$  with the receiving area  $A_{eff}$  is the following:

$$P_{r-NLOS} = IA_{eff}, \quad (10)$$

where  $A_{eff}$  is the effective area of the PD which can be expressed as:

$$A_{eff} = \begin{cases} A_{PD} \cdot \cos \varnothing, & 0 \leq \varnothing < \frac{\pi}{2} \\ 0, & \varnothing \geq \frac{\pi}{2} \end{cases}, \quad (11)$$

where  $\varnothing$  is the irradiance angle on the photodiode.

Finally, the received power can be obtained using the equation:

$$P_r = P_t H_{LOS} + P_{r-NLOS} + N \quad (12)$$

### 3. OFDM system

Figure 3 shows a schematic diagram of an OFDM modulation technique for an Li-Fi system. OFDM signal is generated with a nominal data rate. A serial to parallel conversion for the bit stream is performed and, then mapped to a multilevel modulation such as a 16-quadrature amplitude modulation (QAM). To ensure non-negativity and real OFDM signal output power, as the light source produces incoherent light, the Hermitian symmetry is necessary and the use of a DC bias to guarantee a unipolar signal at the transmitter end, a different optical OFDM has been proposed.

DC optical orthogonal frequency division multiplexing (DCO-OFDM) [14,15] is widely used for realizing the unipolar and non-negative time to the OFDM signal output domain. In DCO-OFDM, the first half of inverse fast Fourier transform (IFFT) input sequences is assigned except the first subcarriers which are set to zero so that the output signal will only consist of positive real values [16,17]. As mentioned before, the Hermitian symmetry is important so

that the output of the IFFT block consists of real-valued signals. Serialization of the information symbols and a cyclic prefix (CP) are added to provide a guard time and compensate the intercarrier interference (ICI). The signal is converted to analogue electrical signals by a digital-to-analogue converter (DAC). A low-pass filter (LPF) is used to remove the aliasing. A LED is modelled to generate a continuous signal.

The free space channel is used to transfer the data from LED to PD at the receiver. Additionally, an optical noise is added due to the ambient light. At the receiver, the received OFDM signals are converted to an electrical signal by using the PD. A DC signal is calculated and removed, and, then, it is filtered by an LPF. The signal is sampled with the analogue-to-digital converter (ADC) at the same sampling rate as the DAC in a transmitter. The CP is removed and serially converted to a digital signal into real data block by a serial-to-parallel (S/P) converter which is applied. The fast Fourier transform (FFT) demodulates the OFDM signal to obtain the  $\frac{N}{2} - 1$  subcarriers, then the subcarriers, which have the necessary information, are removed and, finally, an M-QAM demodulation is performed, and the serial binary data are recovered.

### 4. DFT-S-OFDM system

One of the proposed approaches to minimizing PAPR is DFT-S-OFDM which has been proven one of the most effective methods [5,18,19]. The implementation of the DFT-S-OFDM in Li-Fi will be quite different from the conventional DFT-S-OFDM scheme. The DFT-S-OFDM in Li-Fi systems has rarely been investigated.

Figure 4 shows a diagram of the DFT-S-OFDM scheme for Li-Fi systems. Compared to the conventional OFDM system, there are only few different blue blocks as shown in Fig. 3.

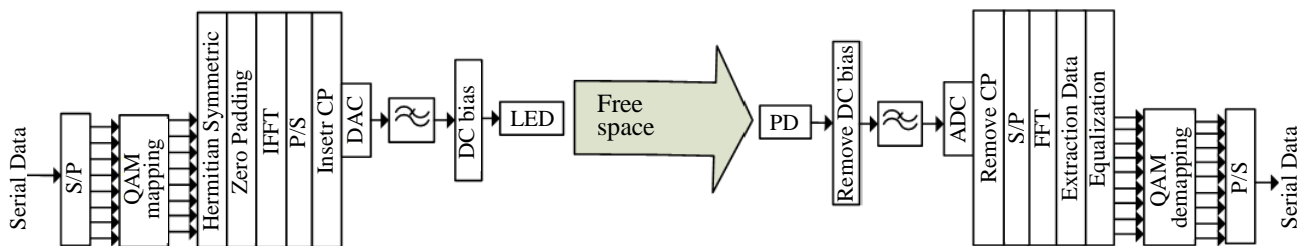


Fig. 3. OFDM system model.

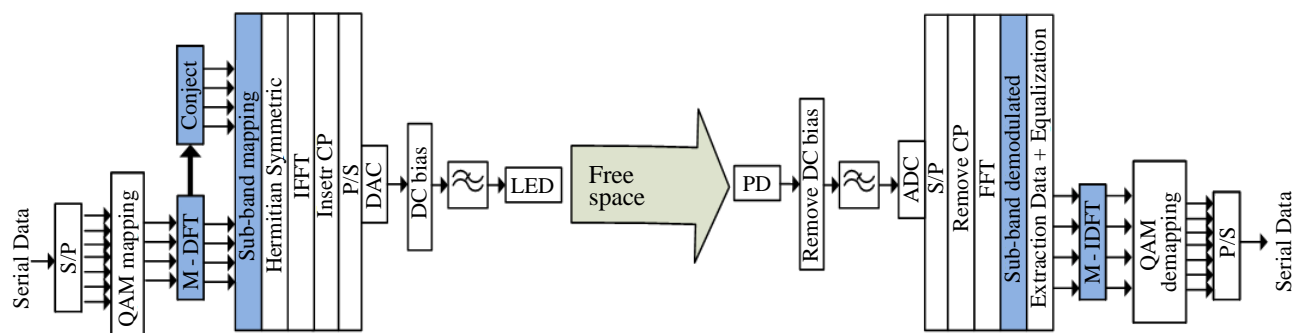


Fig. 4. DFT-S-OFDM system model.

At the transmitter side, parallel data blocks are created by converting serial bits to parallel data blocks. Higher order modulation techniques such as QPSK, 4QAM, and 16QAM are used to map the data. The modulated data  $x_{ik}^m$  are separated into  $m$  sub-bands with  $N$  subcarriers per sub-band in the  $i^{th}$  OFDM symbol. Therefore, the total number of subcarriers of all sub-bands  $K = m \cdot N$ . By applying the  $N$ -point of DFT to each sub-band, the frequency domain is converted.

To generate real baseband DFT-S-OFDM waves, a conjugation operation is added, and, then the Hermitian symmetry is followed. Next, by adding zero subcarriers  $N_{zp}$ , a sub-band mapping is achieved. The  $L$ -point IFFT is used to convert the DFT-spread wave to the time domain from the frequency domain. The DFT-S-OFDM signal is generated by the IFFT where  $L = N_{zp} + m \cdot N$ . Within each OFDM sub-band, the DFT-S-OFDM wave has a low PAPR. In order to provide a guard time and overcome ISI, the last samples of the DFT-S-OFDM symbol are copied to add CP. With DAC, the information symbols are serialized and sampled. A DC bias guarantees a unipolar signal at the end of the transmitter. To filter and remove aliases from the main DFT-S-OFDM signal, an LPF is used. The signal is modulated using LED to generate a continuous signal, and then launched to the free space channel. Additionally, an optical noise is added due to the ambient light. The receiver action is the opposite of the transmitter action. At the receiver, the received DFT-S-OFDM signals are demodulated using the PD.

The DC signal is removed. Then, it is filtered by using the LPF, afterwards the signal is sampled and converted to a digital signal using ADC. The FFT is used to convert the received signal into a frequency domain. Then, FFT extracts the output symbols. Finally, The IDFT is used to convert the frequency symbols to the time domain in the recovered symbols. The traditional DCO-OFDM system is obtained by removing the blue blocks.

The distributed and localized mapping algorithms can be used to accomplish a sub-band mapping of DFT-spread subcarriers [5,19,20].

In the case of distributed DFT-S-OFDM sub-band mapping, the DFT outputs (DDFT-S-OFDM) are inserted within zero subcarriers. There is no equidistance distribution in the zero subcarriers. When the zero subcarriers are distributed evenly amongst the DFT outputs, a particular example of DDFT-S-OFDM is formed, known as the DFT-S-OFDM (IDFT-S-OFDM) interleaved sub-band mapping [21]. The outputs of DFT are padded as successive subcarriers in the localized DFT-S-OFDM (LDFT-S-OFDM) sub-band mapping, considering the zeros inserted at both sides of the IFFT input sequence in the DFT-S-OFDM (LDFT-S-OFDM) [20].

In Ref. 20, it was investigated that the PAPR of IDFT-S-OFDM equals the PAPR of single-carrier systems, while LDFT-S-OFDM has a relatively higher PAPR but still much lower compared to the conventional OFDM. In Li-Fi systems, due to the required real signals, OFDM subcarriers require a special conjugate symmetry constraint [22]. Therefore, the implementation of the DFT-S-OFDM in Li-Fi will be different from the conventional DFT-S-OFDM scheme. The DFT-S-OFDM in Li-Fi systems has rarely been studied [21–23].

In Ref. 22, the provided LDFT-S-OFDM sub-band mapping technique is not accurate, as there are not gaps between all OFDM sub-bands. Therefore, an accurate sub-band mapping for the L-DFT-S-OFDM scheme is presented in this paper. As mentioned before, there are two main models for DFT-S-OFDM such as localized and interleaved models. Figure 5 illustrates two models for Li-Fi systems. The IDFT-S-OFDM inserts subcarriers at a regular interval along the first half of the entire bandwidth and it is important to transmit only the real part of the first subcarrier  $X_0$ . The conjugation subcarriers are added and flipped according to the first half subcarriers with transmitting only the imaginary part of the first subcarrier  $X_0$  which is important to guarantee the real signal. Zeros are added at both sides of subcarriers in the LDFT-S-OFDM scheme. It is not required to insert the real and imaginary parts of the first subcarrier in both halves as the first subcarrier to the input IFFT sequences is zero. The minimum number of LDFT-S-OFDM is 2 sub-bands which are generated by the Hermitian symmetric.

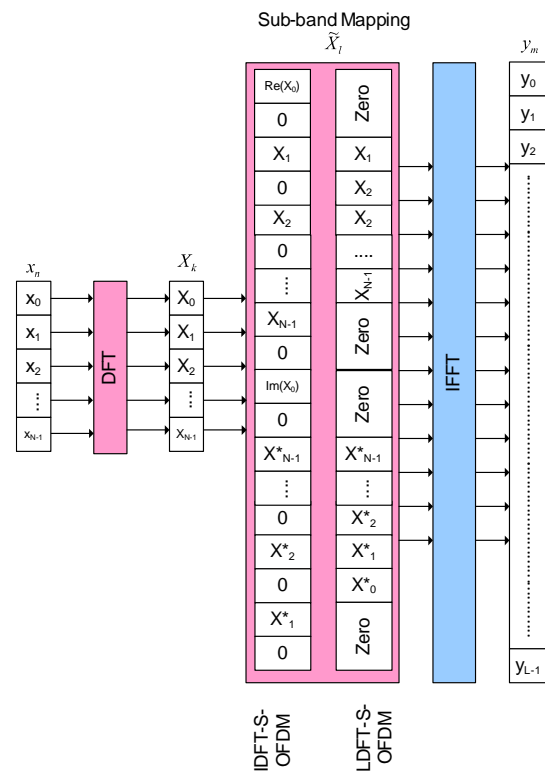


Fig. 5. Signal processing diagram for sub-band techniques for Li-Fi system.

## 5. Results and discussion

OFDM and DFT-S-OFDM signals, and system performance are simulated using Matlab™, with 16QAM, generating a data rate of 150 Mbps and the same spectrum efficiency. The simulation parameters are given in Table 1.

As demonstrated in Fig. 2, the optical wireless communication channel used in simulation is precisely measured using the VLC platform. The simulation results are obtained for the impulse responses of LoS and the first reflection of NLoS channels. Only one LED is used as a transmitter and it is located at the centre of the ceiling of the empty room with one PD which is faced upwards to LED.

Table 1.  
The value of parameters used in simulation.

System Parameters	
Bits per subcarrier	4
FFT/IFFT size	1024
No. of zero padding $N_{ZP}$	512
Number of subcarriers $N_{sc}$	256
CP ratio of the symbol length	0.0625
Data rate	150 Mbps
Sampling rate	150 MHz
A roll off factor of LPF	0.2
LED power	20 Watt
Channel Parameters	
PD Area $A_{PD}$	$10^{-4}$ cm <sup>2</sup>
Semi angle of the half power $\Phi_{1/2}$	70°
Irradiance angle $\Phi_{i,u}$	20°
Incidence angle $\psi_{i,u}$	30°
Semi angle of FOV $\Psi_{max}$	80°
Gain of optical filter and connectors	1
Refractive index of the lens at PD	1.5
Side wall reflectivity	0.8
Floor and coil reflectivity	0.6
Room size	5m×5m×3m
Location of LED	Centre (2.5, 2.5, 3)
Location of PD	(2.5,2.5,0.85)
Distance between LED and PD	2.15 m
DFT-S-OFDM Parameters	
No. of DFT blocks m	2,8,32
DFT size	$N_{sc}/m$

Figure 6 presents the simulated power distribution due to LoS and the first reflection of NLoS channel in the empty room.

The PD is placed on a horizontal plane downwards, 2.15 m from LED and reaches the maximum and minimum power distribution values of 7.16 dBm and 8.51 dBm, respectively.

Figure 7 presents the spectrum band of 8 sub-bands for the LDFT-S-OFDM signal with 4 DFT block diagrams at

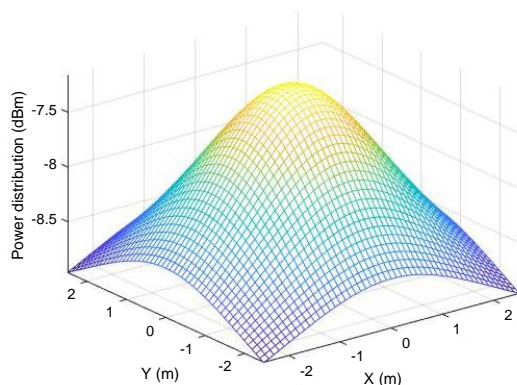


Fig. 6. Power distribution of LED inside an empty room of 5m×5m×3m.

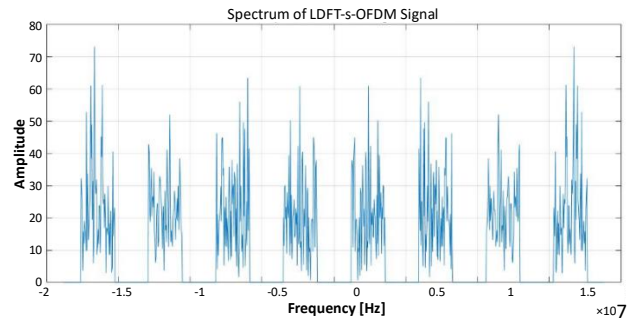


Fig. 7. Spectrum of 8 sub-bands LDFT-S-OFDM signal.

the transmitter. Due to the Hermitian symmetric, the conjugation subcarriers added and flipped the data according to the first half subcarriers which are important to guarantee the real signal. Therefore, 8 sub-bands are generated after FFT. Thus, the minimum number of sub bands which can be obtained in Li-Fi systems using LDFT-S-OFDM scheme is 2 sub-bands.

Figure 8 shows the bit error rate (BER) performance as a signal-to-noise ratio (SNR) function for two DFT-S-OFDM schemes with different sub-bands and DCO-OFDM methods which are used in this simulation for the Li-Fi system.

The required SNRs for a BER of  $10^{-3}$  is 19 dB, 20.6 dB, 21 dB, 22 dB, 22.5 dB, 23 dB, and 23.4 dB for 2 sub-bands of IDFT-S-OFDM, 2 sub-bands of LDFT-S-OFDM, 8 sub-bands of IDFT-S-OFDM, 8 sub-bands of LDFT-S-OFDM, 32 sub-bands of IDFT-S-OFDM, 32 sub-bands of LDFT-S-OFDM, and DCO-OFDM, respectively. The 2 interleaved sub-bands and the localized DFT-S-OFDM schemes can improve SNR at a BER of  $10^{-3}$  by 4.4 dB and 2.8 dB, respectively, compared to the DCO-OFDM system. The computational complexity grows as the number of sub-bands increases, since there are more DFT/IDFT operations in the transmitter and receiver. Also, the phase noise spreads across the entire sub-bands, as does the sub-bands interference, resulting in an

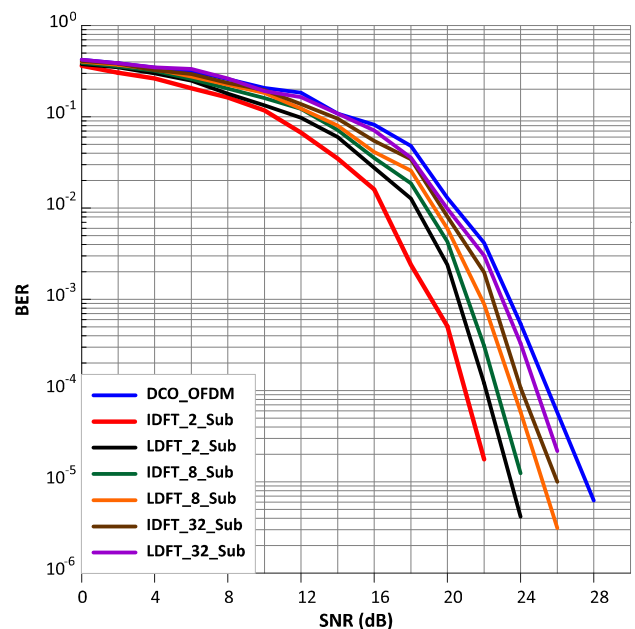


Fig. 8. BER performance as a function in SNR using Li-Fi system.

additional ICI, or inter-block interference. Both DFT-S-OFDM classifications are sensitive to an increasing number of sub-bands, but it still improves the BER performance compared to the DCO-OFDM scheme.

Figure 9 investigates the PAPR performance of DCO-OFDM and two schemes of DFT-S-OFDM with different sub-bands as a function of the complementary cumulative distribution function (CCDF). CCDF is the probability that the PAPR of an OFDM signal is higher than the threshold value  $PAPR_0$ . A DC bias is added to obtain a positive signal after ADC. However, as the DC increases, the signal may be distorted due to the non-linearity of the LED. Therefore, the IDFT-S-OFDM signal yields better PAPR than the LDFT-S-OFDM and DC-OFDM waveforms.

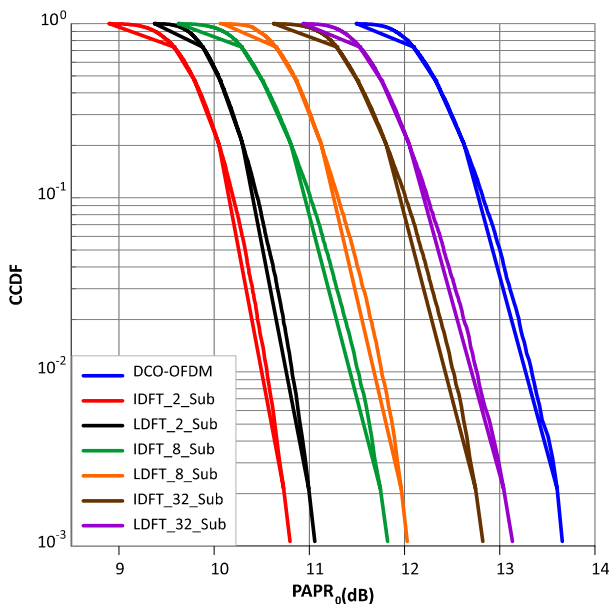


Fig. 9. PAPR vs. CCDF performance using Li-Fi system.

It is clearly observed through the simulation results that for a CCDF of  $10^{-2}$ , a PAPR is required of 10.5, 10.8, 11.4, 11.7, 12.3, 12.6, and 13.1 dB for 2 sub-bands IDFT-S-OFDM, 2 sub-bands LDFT-S-OFDM, 8 sub-bands IDFT-S-OFDM, 8 sub-bands LDFT-S-OFDM, 32 sub-bands IDFT-S-OFDM, 32 sub-bands LDFT-S-OFDM, and DCO-OFDM, respectively. For 2 sub-bands IDFT-S-OFDM, waveform improves the PAPR at a CCDF of  $10^{-2}$  by 2.6 dB compared to the DCO-OFDM signal. The simulation results show that the IDFT-S-OFDM outperforms LDFT-S-OFDM around 0.3 dB and the DFT-S-OFDM scheme significantly mitigates the impact of the PAPR.

## 6. Conclusions

In this paper, the VLC system using a single LED with different DFT-S-OFDM classifications and OFDM methods are discussed. The investigation of the received power characteristic on the available photodiode for the Li-Fi system with LoS and the first reflection of NLoS channel has been clearly explained. To ensure the real signal, a conjugate symmetry constraint is put on the OFDM and DFT-S-OFDM subcarriers due to the Hermitian symmetry. Therefore, the minimum number of sub-bands that can be

obtained in the Li-Fi system using the LDFT-S-OFDM scheme is 2 sub-bands. Increasing the number of sub-bands, the phase noise spreads across the entire sub-bands, as does the interference between the sub-bands, resulting in an additional ICI, or inter-block interference. Both DFT-S-OFDM classifications are sensitive to the increasing number of sub-bands, but still improve performance compared to the DCO-OFDM scheme.

Based on the simulation results, both interleaved and localized DFT-S-OFDM modulations have the lowest error probability compared to the DCO-OFDM technique. At a BER of  $10^{-3}$ , IDFT-S-OFDM and LDFT-S-OFDM schemes with 2 sub-bands can improve SNR by 4.4 dB and 2.8 dB, respectively, compared to the DCO-OFDM system. At a CCDF of  $10^{-2}$ , the PAPR performance of 2 sub-bands of LDFT-S-OFDM and IDFT-S-OFDM formats can improve the PAPR by 2.6 dB and 2.3 dB, respectively, compared to the DCO-OFDM formats in the Li-Fi systems. Therefore, the interleaved and localized DFT-S-OFDM modulation formats are more resistant to channel formats and significantly mitigate the impact of PAPR than the DCO-OFDM modulation technique for the Li-Fi systems.

## Acknowledgement

The authors would like to thank the Egyptian Ministry of Higher Education and Scientific Research for supporting this research proposal

## References

- [1] Armstrong, J. OFDM for optical communications. *J. Light. Technol.* **27**, 189–204 (2009). <https://doi.org/10.1109/JLT.2008.2010061>
- [2] Noé, R. *Essentials of Modern Optical Fiber Communication*. (Springer International Publishing, 2010). <https://doi.org/10.1007/978-3-642-04872-2>
- [3] Sufyan Islim, M. & Haas, H. Modulation techniques for Li-Fi. *ZTE Commun.* **14**, 29–40 (2016).
- [4] DoCoMo, NTT, NEC, SHARP, R1-050702: DFT-spread OFDM with pulse shaping filter in frequency domain in evolved UTRA uplink (2005).
- [5] Myung, H. G., Lim, J. & Goodman, D. J. (2006). Peak-to-average power ratio of single carrier fdma signals with pulse shaping. in *IEEE 17th International Symposium on Personal, Indoor and Mobile Radio Communications 1–5* (IEEE, Helsinki, Finland 2006). <https://doi.org/10.1109/PIMRC.2006.254407>
- [6] Lomba, C., Valades, R. & Duarte, A. Efficient simulation of the impulse response of the indoor wireless optical channel. *Int. J. Commun. Syst.* **13**, 537–549 (2000). [https://doi.org/10.1002/1099-1131\(200011/12\)13:7<8%3C537::AID-DAC455%3E3.0.CO;2-6](https://doi.org/10.1002/1099-1131(200011/12)13:7<8%3C537::AID-DAC455%3E3.0.CO;2-6)
- [7] Haas, H. et al. Introduction to indoor networking concepts and challenges in Li-Fi. *J. Opt. Commun. Netw.* **12**, A190–A203 (2020). <https://doi.org/10.1364/JOCN.12.00A190>
- [8] Alonso-Gonzales, I. et al. Discrete indoor three-dimensional localization system based on neural networks using visible light communication. *Sensors* **18**, 1040 (2018). <https://doi.org/10.3390/s18041040>
- [9] Wu, X., Safari, M. & Haas, H. Access point selection for hybrid li-fi and Wi-Fi networks. *IEEE Trans. Commun.* **65**, 5375–5385 (2017). <https://doi.org/10.1109/TCOMM.2017.2740211>
- [10] Barry, J. R. et al. Simulation of multipath impulse response for indoor wireless optical channels. *IEEE J. Sel. Areas Commun.* **11**, 367–379 (1993). <https://doi.org/10.1109/49.219552>
- [11] Zeng, L. et al. improvement of data rate by using equalization in an indoor visible light communication system. in *4th IEEE International Conference on Circuits and Systems for Communications*. 678–682 (IEEE, Shanghai, China 2008). <https://doi.org/10.1109/ICCSC.2008.149>
- [12] Kahn, J. B. & Barry, J. R. Wireless infrared communications. *Proc. IEEE* **85**, 265–298 (1997). <https://doi.org/10.1109/5.554222>

- [13] Jungnickel, V. et al. A physical model of the wireless infrared communication channel. *IEEE J. Sel. Areas Commun.* **20**, 631–640 (2002). <https://doi.org/10.1109/49.995522>
- [14] Zhan, X. et al. Comparison and analysis of DCO-OFDM, ACO-OFDM and ADO-OFDM in IM/DD systems. *Appl. Mech. Mater.* **701-702**, 1059–1062 (2015). <https://doi.org/10.4028/www.scientific.net/AMM.701-702.1059>
- [15] Zhang, M. & Zhang, Z. An optimum DC-biasing for DCO-OFDM system. *IEEE Commun. Lett.* **18**, 1351–1354 (2014). <https://doi.org/10.1109/LCOMM.2014.2331068>
- [16] Carruthers, J. B. & Kahn, J. Multiple subcarrier modulation for nondirected wireless infrared communication. *IEEE J. Sel. Areas Commun.* **14**, 538–546 (1996). <https://doi.org/10.1109/49.490239>
- [17] Lee, S. H., Jung, S.-Y. & Kwon, J. K. Modulation and coding for dimmable visible light communication. *IEEE Commun. Mag.* **53**, 136–143 (2015). <https://doi.org/10.1109/MCOM.2015.7045402>
- [18] Acolatse K., Bar-Ness, Y. & Wilson, S. K. Novel techniques of single carrier frequency domain equalization for optical wireless communications. *EURASIP J. Adv. Signal Process.* **2011**, 393768 (2011). <https://doi.org/10.1155/2011/393768>
- [19] Myung, H. G., Lim, J. & Goodman, D. J. Single carrier FDMA for uplink wireless transmission. *IEEE Veh. Technol. Mag.* **1**, 30–38 (2006). <https://doi.org/10.1109/MVT.2006.307304>
- [20] Sorger, U., De Broeck, I. & Schnell, M. Interleaved FDMA—a new spread-spectrum multiple-access scheme. in *1998 IEEE International Conference on Communications. Conference Record (ICC). Affiliated with SUPERCOMM'98*. **2**, 1013–1017 (IEEE, Atlanta, USA 1998). <https://doi.org/10.1109/ICC.1998.685165>
- [21] Wu, Z.-Y. et al. Optimized DFT-spread OFDM based visible light communications with multiple lighting sources. *Opt. Express* **25**, 26468–26482 (2017). <https://doi.org/10.1364/OE.25.026468>
- [22] W. Ch., Zhang, H. & Xu, W. On visible light communication using led array with DFT-spread OFDM. in *2014 IEEE International Conference on Communications (ICC)* 3325–3330 (2014) (IEEE, Sydney, Australia 2014). <https://doi.org/10.1109/ICC.2014.6883834>
- [23] Puntsri, K. & Ekkaphol, K. Experimental comparison of OFDM SC-FDM and PAM for low speed optical wireless communication systems. In *7th International Electrical Engineering Congress (iEECON)* 1–4 (IEEE, Hua Hin, Thailand 2019). <https://doi.org/10.1109/iEECON45304.2019.8938969>